Transaction B: Mechanical Engineering
Vol. 16, No. 4, pp. 363–369

Research Note

SCIENTIA IRANICA

Effect of Different Geometries in Simulation of 3D Viscous Flow in Francis Turbine Runners

B. Firoozabadi[1,*], R. Dadfar[1], A.P. Pirali[1] and G. Ahmadi[2]

Abstract. *Overall turbine analysis requires large CPU time and computer memory, even in the present days. As a result, choosing an appropriate computational domain accompanied by a suitable boundary condition can dramatically reduce the time cost of computations. This work compares different geometries for numerical investigation of the 3D flow in the runner of a Francis turbine, and presents an optimum geometry with least computational effort and desirable numerical accuracy. The numerical results are validated with a GAMM Francis Turbine runner, which was used as a test case (GAMM workshop on 3D computation of incompressible internal flows, 1989) in which the geometry and detailed best efficiency measurements were publically accessible. In this simulation, the flow is assumed to be steady and the inlet boundary condition is prescribed using experimental data. The effect of turbulence is considered by the $k-\varepsilon$ model. The present investigation demonstrates that consideration of 2-blade geometry with periodic boundary conditions is the best choice of computational domain. By 1-blade geometry, convergence of the numerical simulation is not appropriate, whereas 13-blade geometry leads to a coarse grid that can increase inaccuracy and computational cost. Finally, this paper presents a qualitative survey to forecast cavitation region inception which correlates satisfactorily with experimental observations.*

Keywords: *Numerical simulation; Francis turbine runner; GAMM; Viscous flow analysis.*

INTRODUCTION

Since the advent of the industrial revolution, worldwide energy consumption has been growing steadily, makeing it important (unavoidable) to exploit already existing energy to the fullest extent. Hydropower energy as a renewable, reliable and cost effective energy source has many benefits over other energy sources, which makes the study and development of this technology inevitable. The high cost of experimental studies along with the rapid increase in computer power provides valuable opportunities for the numerical investigation of flowing fluid through turbomachines. For a Francis turbine, the flow enters stay vanes after passing through the spiral case, then guide vanes conduct the water tangentially to the runner. This radial flow acts on the runner vanes, causing the runner to spin. Complex and rotating geometry, the curvature of the flow passage along with vortex generation, cavitation and the unsteady nature of flow in the runner are some instances of difficulties in the analysis of a runner. It is, however, the most significant part of the hydraulic turbine, inaccurate design of which can lead to a remarkable head loss and notable decrease in efficiency.

Up to now, the analysis of 3D flow through the runner of a Francis turbine was carried out using a single runner blade passage and inviscid flow assumption, which can approximately predict results under the best efficiency operation condition [1]. However, taking into account viscous effects can make results much more accurate. In most works, steady and viscous flow with a proper turbulent model is simulated through a single passage of the runner [2]. Some works presented simulation of a complete runner [3] and other works attempted to couple the whole system by using a special algorithm from the inlet of the spiral casing to the outlet of the draft tube [4-6]. Recently, some attempts have been made to simulate a complete Francis turbine using parallel processing techniques [7].

1. *Department of Mechanical Engineering, Sharif University of Technology, Tehran, P.O. Box 11155-956, Iran.*
2. *Department of Mechanical and Aeronautical Engineering, Clarkson University, Potsdam, NY, USA.*
*. *Corresponding author. E-mail: firoozabadi@sharif.edu*

Received 24 July 2007; received in revised form 6 July 2008; accepted 11 May 2009

In designing a runner, having the proper means with the ability to present a quick and accurate simulation of the flow seems to be crucial. In this paper, it is proved that engineers can optimize their projects with the aim of a commercial code, which is publically available. This work presents a numerical simulation of 3D flow for a GAMM Francis turbine under the best efficiency operating conditions for different computational domains, by implementing a commercial code: Fluent. After choosing several geometries, the best geometry with the most precise results and minimum computational time cost are presented. The computational domain begins from the inlet of the runner and ends at the inlet of the draft tube. Numerical results are compared with the experimental measurements of a GAMM turbine for validation.

NUMERICAL ANALYSIS

For all calculations, a three-dimensional viscous flow analysis in a Cartesian coordinate system and a moving reference frame based on averaged Navier-Stokes equations has been applied. In addition, the two equation standard $k-\varepsilon$ model is adopted as a closure form. Moreover, in the present numerical simulation, using Fluent code, a finite volume method with a SIMPLEC algorithm for pressure-velocity coupling, a power law scheme as the convection discretization procedure, and a collocated grid arrangement are used. As a convergence criterion, we ran the computations to the point where the scale residuals were less than 10^{-6} for all equations.

Turbulence Modeling

The standard $k-\varepsilon$ model with a logarithmic wall function to treat near wall regions is used in the present work. The standard $k-\varepsilon$ model is a semi-empirical model based on the transport equations for turbulence kinetic energy (k) and its dissipation rate (ε). This model is used for a wide range of difficult problems, but for cases that include inhomogeneous turbulent and non-equilibrium effects, using this model made some extra diffusive results. This model predicts a small vortex for separated flows. In addition, the turbulence modeling in swirling flows is more complex due to the body force created by the swirl. However, this model is less computationally expensive, seems to be proper for the runner's best efficiency operating point and was well validated with experimental data [4]. Of course, some studies were made by the Shear Stress Transport (SST) model, which is a change from the standard $k-\omega$ model (in the inner region of the boundary layer) to a high-Reynolds-number version of the $k-\varepsilon$ model in the outer region of the boundary layer. But, the $k-\varepsilon$ model was finally preferred.

Moving Reference Frame Treatment

Fluent software allows one to solve rotating frame problems using either the absolute velocity, $\vec{V}$, or the relative velocity, $\vec{V}_r$, as the dependent variable. The two velocities are related by the following equation:

$$\vec{V}_r = \vec{V} - (\vec{\Omega} \times \vec{r}). \tag{1}$$

Here, $\vec{\Omega}$ is the angular velocity vector (i.e. the angular velocity of the rotating frame), $\vec{r}$ is the position vector in the rotating frame, and $\vec{\Omega} \times \vec{r}$ is the centrifugal acceleration. Finally, using a relative velocity formulation, the left side of the momentum Equation 3 in vector notation reads:

$$\nabla.(\rho \vec{V}_r \vec{V}_r) + \rho(2\vec{\Omega} \times \vec{V}_r + \vec{\Omega} \times \vec{\Omega} \times \vec{r}),$$

where $\rho(2\vec{\Omega} \times \vec{V}_r)$ is the Centrifugal Force [7].

Governing Equations

The time-averaged continuity and Navier-Stokes equations for incompressible flow are as follows:

$$\frac{\partial}{\partial x_i}(\rho U_i) = 0, \tag{2}$$

$$\frac{\partial}{\partial x_j}(\rho U_i U_j) = -\frac{\partial p}{\partial x_i} + \frac{\partial}{\partial x_j}\left[(\mu + \mu_t)\frac{\partial U_i}{\partial x_j}\right] + \rho g_i. \tag{3}$$

The standard $k-\varepsilon$ model for the turbulent kinetic energy, k, and the dissipation rate, ε, are:

$$\frac{\partial}{\partial x_i}(\rho k U_i) = \frac{\partial}{\partial x_i}\left[\left(\mu + \frac{\mu_t}{\sigma_k}\right)\frac{\partial k}{\partial x_i}\right] + G_k - \rho\varepsilon, \tag{4}$$

$$\frac{\partial}{\partial x_i}(\rho \varepsilon U_i) = \frac{\partial}{\partial x_j}\left[\left(\mu + \frac{\mu_t}{\sigma_\varepsilon}\right)\frac{\partial \varepsilon}{\partial x_j}\right] + C_{1\varepsilon}\frac{\varepsilon}{k}G_k - C_{2\varepsilon}\rho\frac{\varepsilon^2}{k}, \tag{5}$$

where the terms are defined as:

$$G_k = \mu_t(2S_{ij}S_{ij}), \tag{6}$$

where G_k represents the production of turbulence kinetic energy due to the mean velocity gradient, and the mean strain rate is $S_{ij} = 1/2\left(\frac{\partial U_i}{\partial x_j} + \frac{\partial U_j}{\partial x_i}\right)$.

Coefficients $C_{1\varepsilon}$ and $C_{2\varepsilon}$ are constants and σ_k and σ_ε are the turbulence Prandtl numbers for k and ε, respectively. The turbulent (or eddy) viscosity, μ_t, is computed by combining k and ε as follows:

$$\mu_t = \rho C_\mu \frac{k^2}{\varepsilon},$$

where C_μ is a constant.

$$\sigma_k = 1.0, \qquad \sigma_\varepsilon = 1.3, \qquad C_{1\varepsilon} = 1.44,$$

$$C_{2\varepsilon} = 1.92, \qquad C_\mu = 0.09. \tag{7}$$

Geometry

Due to the significance of the flow analysis through hydraulic turbines, some benchmarks have been developed in the world. One of them is the GAMM Francis turbine workshop, which is publicly available and used in this paper. Figure 1 shows the GAMM Francis turbine view [8]. This turbine is a medium/high specific turbine with specific speed 0.5. The computational domain was built based on the GAMM turbine, which begins with the conical surface generated by the BB' axis and ends with the disc of radius DD' (Figure 1). The BB' axis conventionally marks the runner inlet, while the DD' axis corresponds to the draft tube inlet. The chief difficulty of the runner computational domain consists in building the strong curved 3D runner blade surface.

As mentioned above, the periodic flow assumption for the best efficiency operating point satisfies the physics of this problem.

Four different geometries have been used in the present work. The first geometry, {1}, includes one blade. In this case, the 3D computational domain is obtained by subtracting one-blade solid from 1/13 runner solid. The second geometry, {2}, includes 2/13 runner solid. The third, {3}, and fourth, {4}, geometries include the total runner with and without a draft tube. These geometries were shown in Figure 2 (a-d).

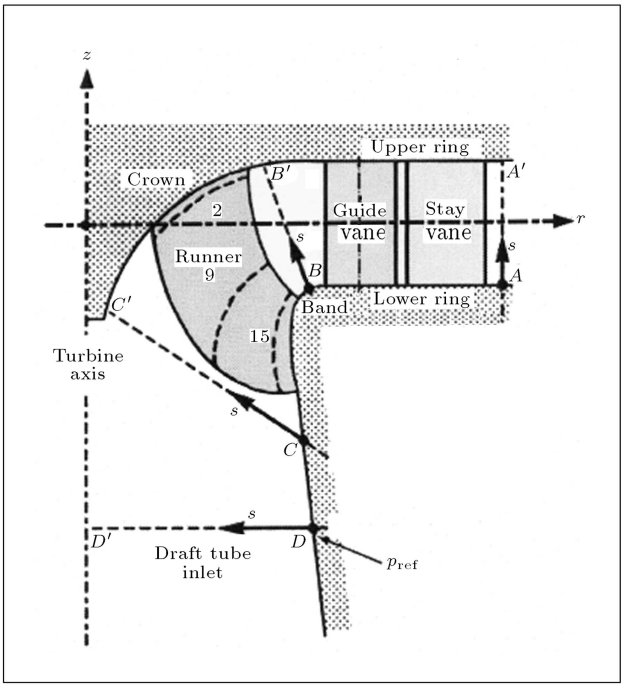

Figure 1. GAMM Francis turbine runner [8].

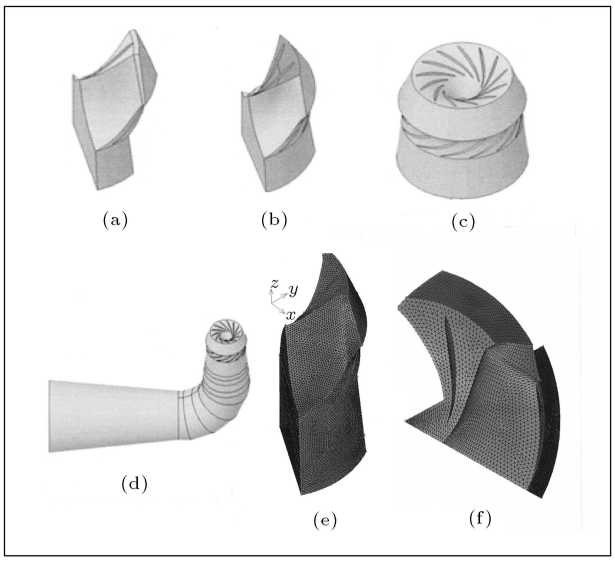

Figure 2. Three-dimensional computational domain: a) Geometry {1}, b) Geometry {2}, c) Geometry {3}, d) Geometry {4} e and f) Unstructured mesh for geometry {1}.

Grid Generation

The 3D computational domain is discretized using an unstructured grid and tetrahedral mesh (Figure 2e). The grids have been generated using the FLUENT preprocessor, Gambit.

Boundary Conditions

Inlet

Data corresponding to the actual velocity field measured at the runner inlet, axis BB', was prescribed on the inlet conical surface (Figure 3).

In this boundary, the turbulence intensity (the ratio of the root-mean-square of the velocity fluctuations to the mean flow velocity) and turbulence length scale were considered as 8% and 0.02 m, respectively. The relationship between turbulence intensity, ℓ, and turbulence kinetic energy, k and ε, are as follows:

$$k = \frac{3}{2}(u_{\text{avg}} I)^2,$$

$$\varepsilon = C_\mu^{3/4} \frac{k^{3/2}}{\ell},$$

where u_{avg} is the mean flow velocity and C_μ is an empirical constant specified in the turbulence model, as mentioned above.

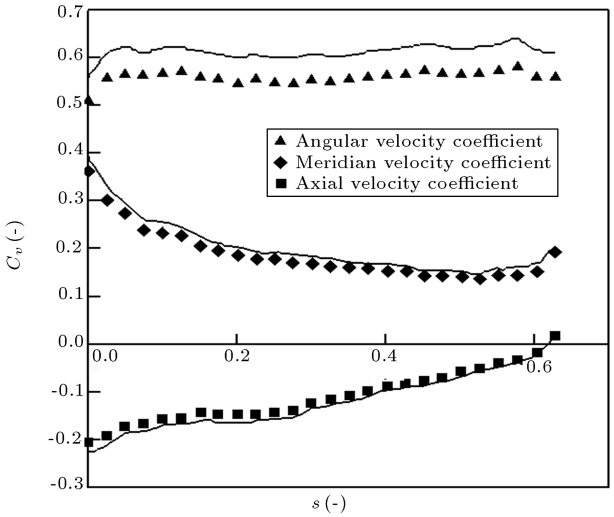

Figure 3. Velocity coefficients on the runner inlet axis BB': Solid lines: Computational results; Symbols: Experimental data.

Outlet

The radial equilibrium condition was chosen on the outlet disc. Such a condition can be devised by assuming that, in this section, there is no radial flow, i.e. $v_r = 0$. The momentum equation yields:

$$\frac{\partial p}{\partial r} = \frac{\rho V_\theta^2}{r}. \tag{8}$$

Then, in this boundary, the pressure gradient was prescribed equal to radial acceleration. In addition, on the outlet disk, the backflow turbulence intensity and backflow turbulence length scale were considered constants, 10% and 0.02 m, respectively.

Periodic

For the first and second geometry (1-blade and 2-blade geometries), the periodical conditions were imposed on the periodic boundary:

$$\vec{V}(r,\theta,z) = \vec{V}\left(r,\theta+\frac{2\pi}{Z},z\right),$$

and:

$$p(r,\theta,z) = p\left(r,\theta+\frac{2\pi}{Z},z\right). \tag{9}$$

Indeed, there is no difference between the periodicity of the flow in the boundaries of 1- and 2-blade geometries and we can impose the periodic condition on two sides of these two geometries. We will see in the next part that this boundary condition improves the matching between physics and computation.

Wall

These boundaries are hub, crown, shroud and blades. A standard wall function, which has been most widely used for industrial flow, was imposed on the wall boundaries in this work. The log-law is employed when $y^* > 11.225$ and when the mesh was such that $y^* < 11.225$ at the wall-adjacent cells, the laminar stress-strain relationship was applied. It should be noted that, in the Fluent software, the laws-of-the-wall for the mean velocity are based on the wall unit [9],

$$y^* = \frac{C_\mu^{1/4} k_p^{1/2} y_p}{\mu}. \tag{10}$$

GAMM FRANCIS TURBINE

Geometry

The test model, which corresponds to a Francis turbine of medium/high specific speed, was designed at the Hydraulic Machines and Fluid Mechanics Institute (IMHEF) for experimental research studies in the hydraulic laboratory. The model was used as a test case in the 1989 GAMM workshop, where all geometrical information and the best efficiency measurements were available. The runner has 13 blades and its external diameter is 0.4 m, so the reference radius is $R_{\text{ref}} = 0.2$ m. The runner geometry was defined by 17 profiles (Figure 4).

The detailed measurements for the best efficiency operating point ($\varphi = 0.286$, $\psi = 1.07$, $\eta = 0.92$) were

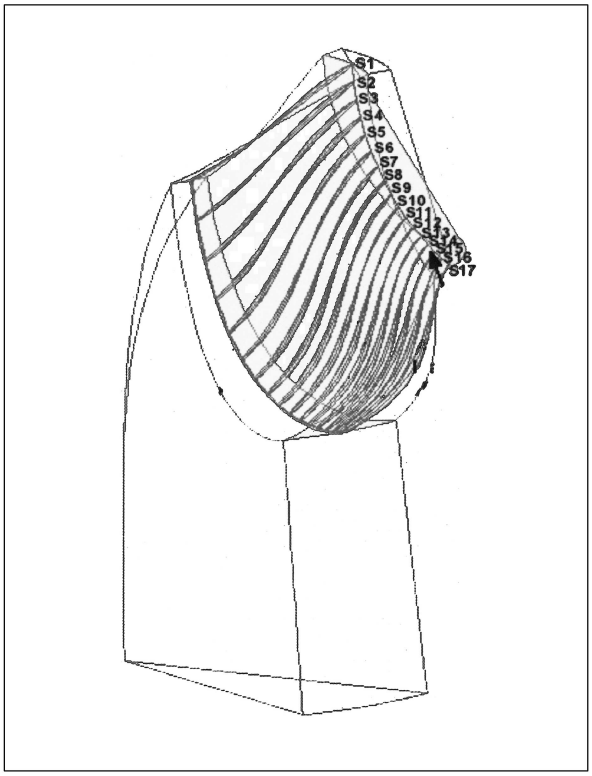

Figure 4. 17 sections for the geometrical description of the Francis turbine blade.

available for the GAMM workshop. The database was comprised of the integral properties of the flow such as the global volume flow rate ($Q = 0.372$ m^3/s) and detailed pressure and velocity distribution measurements on some specified axes. The runner measurement axes are shown in Figure 1. The measured BB' axis, making an angle of 20 degrees with the vertical, was imposed as the inlet boundary condition in this work. In the present work, the numerical results have been validated with measured data on CC' and DD' axes. The CC' axis is located just under the trailing edge of the blades and the DD' axis is located in the outlet of the runner. The CC' axis makes an angle of 55 degrees with the vertical and intersects the shroud at $R = 205.09$ mm and $Z = -208.47$ mm. The DD' axis is horizontal and intersects the shroud at $R = 218.38$ mm and $Z = -346.35$ mm [10].

Measurements

According to the published data of the GAMM workshop, measurements were made using a 6 mm diameter five-hole pressure probe, which gives the three components of the local flow components and the local static pressure. The flow behavior at the outlet of the draft tube did not allow for detailed measurements with the available instrumentation because of flow instabilities [2].

VALIDATION OF THE COMPUTATIONAL RESULTS

Velocity Field

Figure 5 compares computed velocity profiles with the measurement data for the geometries {1} and {2}. The flow angle has not been presented because validation of the comput velocity component means validation of the computed flow angles, and these two quantities are in close relation.

Figure 5 shows measurements of geometry {1} in the left and geometry {2} in the right side. As mentioned above, geometry {1} includes one blade, while geometry {2} includes two blades. The top figures indicate the normalized velocity at the CC' axis and the lower ones demonstrate results at the measured DD' axis, which were described in previous sections. The normalized abscissa, s, is defined as the distance

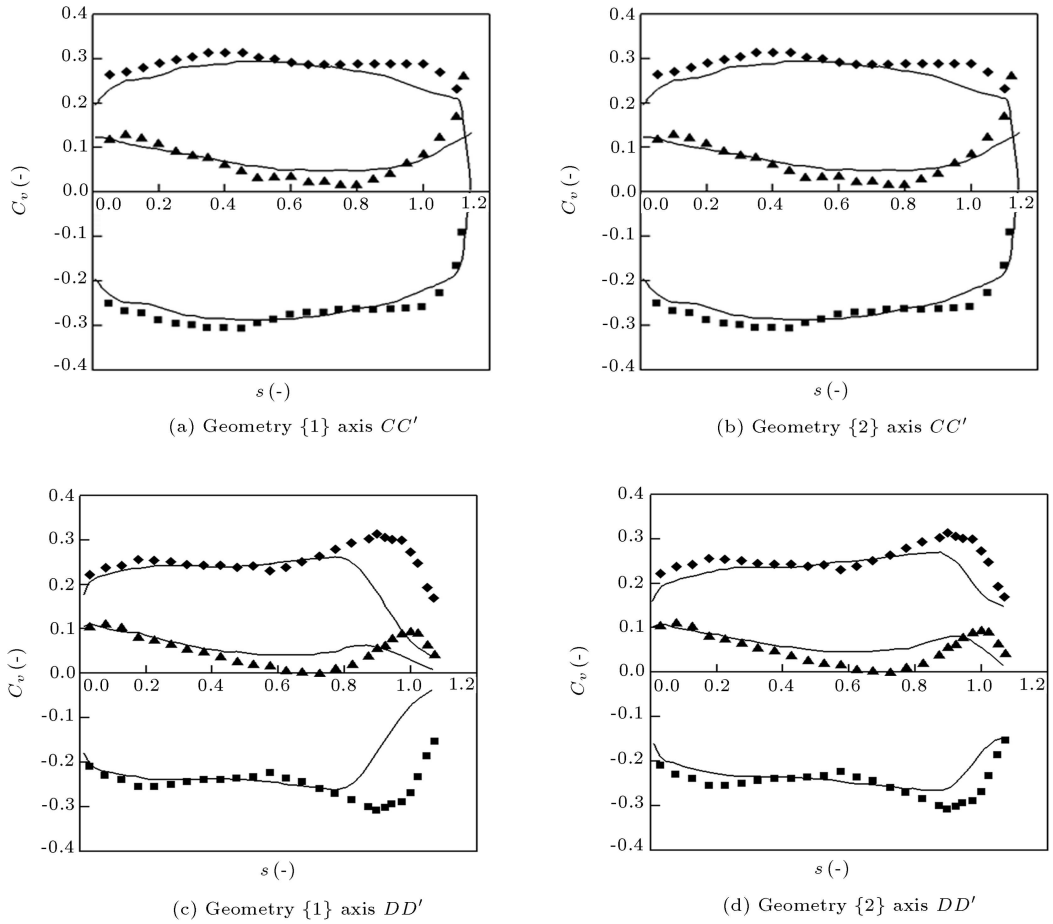

(a) Geometry {1} axis CC'

(b) Geometry {2} axis CC'

(c) Geometry {1} axis DD'

(d) Geometry {2} axis DD'

Figure 5. Normalized velocities; Solid lines: computational and experimental results; ■: axial, ♦: meridian, ▲: angular.

from the shroud aligned with the measurement axis, normalized by the reference radius, $R_{\text{ref}} = 0.2$ m. The velocities are normalized with $\sqrt{2E}$, where E is the specific hydraulic energy of the computational domains, C_r is the radial normalized velocity coefficient, C_z is the axial velocity coefficient, $C_v = \sqrt{C_r^2 + C_z^2}$ is the meridian absolute velocity coefficient, and markers are the measured values.

The computational results show that the velocity distributions agree fairly well with the measured axes CC' and DD' for 2-blade geometry (right figure). But, at the measured axis DD', the results show that 1-blade geometry (left figure) disagrees with the measured data in the central region of the runner (large s).

As an exercise, the problem was solved by two different grids for each of the geometries, which are discretized using between 125 and 300 thousand finite volumes (cells). Results show that the time of convergence for 2-blade geometry is significantly less than that for 1-blade geometry. This means that computational cost decreases by choosing two-blade geometry. Figure 6 shows the comparison between the time expenditure of one and two-blades that is needed for convergence. As seen in these two figures (5 and 6), with constant grid density for the 1- and 2-blade computational domain, the time needed for convergence for two-blade geometry with more grids is less than for one-blade geometry. In addition, the computational errors are less in two-blade geometry. It seems that the reason is the larger, well posed region in this geometry that better satisfies the physics of the flow. Indeed, we decrease the Neumann condition and replace the like- Dirischlet condition.

Figure 7 compares the computed velocity profiles with the measurements for geometries {3} and {4}.

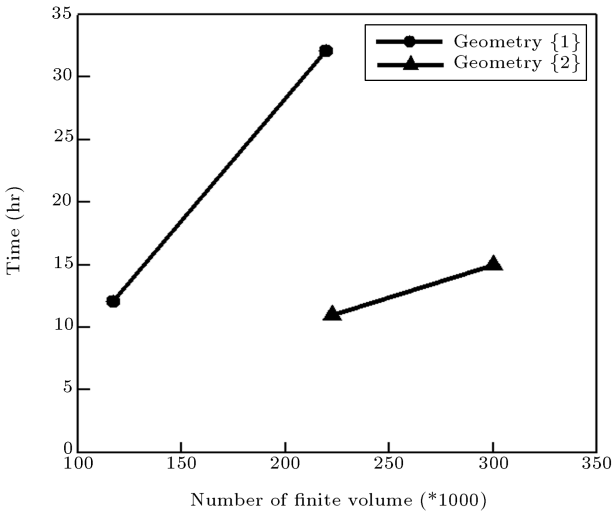

Figure 6. Time cost of convergence per number of finite volume (a domain is divided into a number of finite volumes or cells).

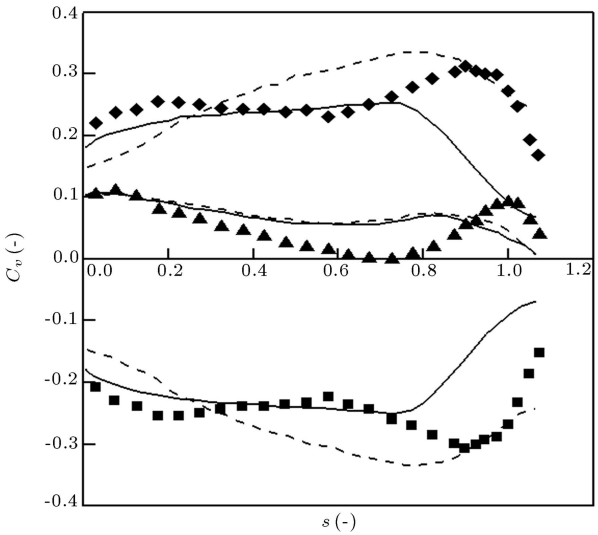

Figure 7. Circumferentially averaged computational results. Solid lines: Geometry {3}, Dashed lines: Geometry {4}. Experimental data: ■: axial, ♦: meridian, ▲: angular.

Dashed lines are the numerical data of the geometry with a draft tube. Geometry {4} includes a draft tube and the computations show that in some regions, geometry {3} matches better with the experiments and in some regions geometry {4}. Of course, because these two cases have large computational domains, their meshes are very coarse and the results are not reliable, but this exercise shows that ignoring the draft tube does not cause a significant error in the numerical simulation.

Cavitation Development Region

A qualitative comparison between the numerical visualization of the cavitation region (Figure 8a) and the photography of the experimental visualization (Figure 8b) is presented. From the computation, it can be seen that the cavitation inception region appears on the suction side of the Francis runner blade, in the neighborhood of

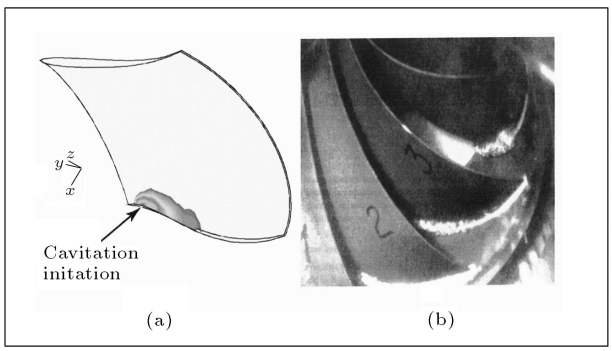

Figure 8. a) Computed cavitational zone development; b) Photography of the inlet edge cavitation development [9].

the leading edge and close to the band. The blue spot indicates that the lowest pressure is well in agreement with the laboratory observation.

CONCLUSION

This work compares several different geometries for numerical investigation of 3D flow in the runner of a Francis turbine, and suggests an optimum geometry whose numerical simulations can lead to desirable results with least computational effort. Based on the consequences of numerical simulations in several computational domains including a complete runner with a draft tube, a complete runner and a runner with 1 and 2 blades, it is concluded that the time cost of computation can reduce dramatically by choosing a two-blade geometry of a runner with periodic boundary conditions, while considering that a single blade passage can result in inappropriate convergence and that 13 blades, with and without a draft tube, lead to course grids and intensive computation.

Furthermore, a qualitative comparison between the numerical visualization of the cavitation region and the photography of the experimental visualization shows that the cavitation inception region appears on the suction side of the Francis runner blade, in the neighborhood of the leading edge and close to the band, and can be predicted satisfactorily by the present numerical simulation.

NOMENCLATURE

$C_v{=}c_v/\sqrt{2E}$ $= \sqrt{C_r^2 + C_z^2}$	absolute meridian velocity coefficient (-)
$C_r = c_r/\sqrt{2E}$	absolute radial velocity coefficient (-)
$C_z = c_z/\sqrt{2E}$	absolute axial velocity coefficient (-)
$E = gH$	specific hydraulic energy (J/kg)
H	net head
$Ns = \frac{\Omega(r/\min)\sqrt{bhp}}{[H(ft)]^{5/4}}$	specific speed (-) (bhp: brake horsepower)
P	static pressure (N/m^2)
Q	volume flow rate (m^3/s)
$R_{\text{ref}} = 0.2$ m	reference radius (m)
k	turbulent kinetic energy (m^2/s^2)
ε	dissipation rate (m^2/s^2)
$s = \text{length}/R_{\text{ref}}$	normalized abscissa (-)
$\eta = T\Omega/\rho$ QE	efficiency (-)
Ω	angular rotation (s^{-1})
$\varphi = Q/\pi\Omega R^3$	volume flow coefficient (-)
$\Psi = 2E/\Omega^2 R^2$	energy coefficient (-)

REFERENCES

1. Vu, T.C., Keon, k., Coulson S., Neury C. and Winkler S. "A comparative study of computational methods for a high specific speed Francis runner flow analysis", *Proceedings XVII IAHR Symposium*, Beijing (1994).
2. Nilsson, H. and Davidson, L. "A validation of parallel multiblock CFD against the GAMM Francis water turbine runner at best efficiency and off-design operating conditions", Publication 02/05, Chalmers University of Technology, Göteborg, Sweden, p. 42 (2001).
3. Cobut, D. et al. "A numerical study of the flow in a Francis turbine runner at off-design operating conditions", *Conference on Modeling, Testing & Monitoring for Hydro Power Plants-II*, IMHEF Report T-96-14 (1996).
4. Muntean, S., Ruprecht, A., Susan-Resiga, R. "Development of a swirling flow apparatus for analysis and development of swirling flow control", *3rd German-Romanian Workshop on Turbomachinery Hydrodynamics*, May 10-12, Timisoara, Romania (2007).
5. Muntean, S. "Numerical methods for the analysis of the 3D flow in Francis turbine runners", PhD Thesis, Politechnica University of Timisoara, Romania (2002).
6. Muntean, S., Susan-Resiga, S. and Anton, I. "3D flow analysis of the GAMM Francis turbine for variable discharge", in *Proceedings of the 21st IAHR Symposium on Hydraulic Machinery and Systems*, Avellan, F., Ciocan, G. and Kvicinsky, S., Eds., Lausanne, Switzerland, **1**, pp. 139-146 (2002).
7. Ruprecht, A., Heitele, M. and Helmrich, T. "Numerical simulation of a complete Francis turbine for variable discharge", *Proceedings XXI IAHR Symposium*, Lausanne (2002).
8. Parkinson, E. "Test case 8: Francis turbine", *Turbomachinery Workshop ERCOFTAC II* (1995).
9. FLUENT 6, "User's Guide", *Fluent Incorporation* (2001).
10. Avellan, F., Dupornt, P., Farhat, M., Gindroz, B., Henry, P., Hussain, M., Parkinson, E. and Santal, O. "Flow survey and blade pressure measurements in a Francis turbine model", *Proceedings of 15th IAHR Symposium on Modern Technology in Hydraulic Energy Production*, Belgrade (1990).